

## Discovery of Rapid Polarization Angle Variation During the 2022 Outburst of XTE J1701-462

QING-CHANG ZHAO,<sup>1,2</sup> HONG LI,<sup>1</sup> LIAN TAO,<sup>1</sup> AND HUA FENG<sup>1</sup>

<sup>1</sup>Key Laboratory of Particle Astrophysics, Institute of High Energy Physics, Chinese Academy of Sciences, Beijing 100049, China

<sup>2</sup>University of Chinese Academy of Sciences, Chinese Academy of Sciences, Beijing 100049, China

### ABSTRACT

The geometry of the Comptonization corona in neutron star low-mass X-ray binaries is still unclear. We conducted time-resolved polarimetric analysis of the archival observations of XTE J1701–462 obtained with the *Imaging X-ray Polarimeter Explorer* during its 2022 outburst, and found that the polarization angle (PA) varied significantly with time when the source was in the normal branch (NB), with  $67 \pm 8^\circ$  in the first epoch,  $-34 \pm 8^\circ$  in the second, and  $-58 \pm 8^\circ$  in the third, last epoch. Meanwhile, the polarization degree remained constant at around 2%, above the minimum detectable polarization at the 99% confidence level ( $\text{MDP}_{99}$ ). The rapid PA variation causes depolarization in the time-averaged data, resulting in a nondetection as reported in the literature. The rapid (intra-day) PA variation may suggest that there is a fast transformation of the corona geometry, likely switching from a slab geometry to a more vertically extended spreading layer geometry, along with enhanced disk emission and reflection.

### 1. INTRODUCTION

Neutron star low mass X-ray binaries (NS-LMXBs) are powered by weakly magnetized (typically  $10^7 - 10^9$  G) neutron stars accreting matter from a companion star. A widely used classification scheme for NS-LMXBs is based on their evolutionary tracks in the color-color diagrams (CCD) and/or the hardness-intensity diagrams (HID; [Hasinger & van der Klis 1989](#); [van der Klis 1989](#)). According to the shape of evolutionary tracks, the sources can be classified into two subclasses: ‘Z’ sources or ‘Atoll’ sources.

The X-ray emission from NS-LMXBs generally consists of two spectral components: a soft thermal component and a hard Comptonization component. The soft component can be modeled as a multicolor disk blackbody with an innermost disk temperature of  $\lesssim 1$  keV. The hard Comptonization component is produced in a relatively cool corona (2–3 keV) likely located in the transition layer (or boundary layer), a region between the Keplerian accretion disk and the surface of neutron star ([Shakura & Sunyaev 1988](#); [Popham & Sunyaev 2001](#)). Frequency-resolved X-ray spectroscopy suggests that the short-term X-ray variability mainly orig-

inates in this region ([Gilfanov et al. 2003](#)). The geometry of the transition layer is unclear (for reviews see [Done et al. 2007](#); [Di Salvo et al. 2023](#)). For example, it is proposed that a spreading layer over the neutron star surface will form when the accretion rate is high ([Inogamov & Sunyaev 1999](#); [Suleimanov & Poutanen 2006](#)). It is argued that X-ray spectro-polarimetry is capable of resolving the geometry of transition layer ([Farinelli et al. 2024](#)).

Sco X-1 is the first NS-LMXB observed with X-ray polarimetry; both OSO-8 ([Novick et al. 1977](#)) and PolarLight ([Feng et al. 2019](#)) found a polarization angle (PA) in line with the orientation of radio jet ([Long et al. 1979, 2022](#)), which is presumably the symmetric axis of the inner accretion flow. The *Imaging X-ray Polarimetry Explorer* (*IXPE*; [Soffitta et al. 2021](#); [Weisskopf et al. 2022](#)) found a similar result in Cyg X-2 that the PA is aligned with the radio jet ([Farinelli et al. 2023](#)). However, the *IXPE* observation of Sco X-1 detected a distinct PA, suggestive of a variable emitting geometry probably related to the emission state. In Cir X-1, the PA was found to vary with both time and hardness ratio, by  $67^\circ \pm 11^\circ$  between the states with the lowest and highest hardness ratios ([Rankin et al. 2024](#)), indicative of a synchronous change in emitting geometry and spectrum. Notably, GX 13+1 exhibited a continuous rotation of PA by  $70^\circ$  over a course of two days, along with a significant variation in the polarization degree (PD); however, no significant spectral changes were identified ([Bobrikova et al. 2024](#)). A PD variation was observed in both GX 5-1 ([Fabiani et al.](#)

lihong02@ihep.ac.cn

taolian@ihep.ac.cn

hfeng@ihep.ac.cn

2024) and XTE J1701–462 (Cocchi et al. 2023; Jayasurya et al. 2023; Yu et al. 2024) while the PA remained constant; also see Ursini et al. (2024) for a recent review.

XTE J1701–462 is a transient NS-LMXBs that was first discovered with the All-Sky Monitor (ASM) onboard the *Rossi X-ray Timing Explorer (RXTE)* on January 18, 2006 (Remillard et al. 2006). This source is unique because it displays characteristics of both Z-type and Atoll-type sources (Homan et al. 2007; Lin et al. 2009b). The distance to XTE J1701–462 is estimated to be 8.8 kpc with an uncertainty of 15%, based on the photospheric radius expansion of type-I bursts (Lin et al. 2009a). Furthermore, the absence of eclipses or absorption dips constrains the orbital inclination to be less than  $75^\circ$  (Lin et al. 2009b).

XTE J1701–462 underwent a new outburst in September 2022 (Iwakiri et al. 2022), during which the source was observed with *IXPE* (Cocchi et al. 2023; Jayasurya et al. 2023), with a high PD of approximately 4.6% in the horizontal branch (HB). However, the polarization was undetected when the source entered the normal branch (NB), with a 99% PD upper limit of 1.5%. Yu et al. (2024) reanalyzed the data and obtained consistent results.

In this work, we analyzed the archival *IXPE* data of XTE J1701–462 and discovered a significant PA variation in the second observation when the source was in the NB. The paper is organized as follows. Details about the observations and data reduction are described in Section 2. The results are presented in Section 3 and discussed in Section 4.

## 2. OBSERVATIONS AND DATA REDUCTION

The source was observed with *IXPE* in the HB on 2023-09-29 (ObsID 01250601; Obs1) and in the NB on 2023-10-08 (ObsID 01250701; Obs2), see Figure 1 for the CCD and HID in the two observations.

Our analysis begins with the level-2 data, which are further reduced and analyzed using *ixpeobssim* v31.0.1 (Baldini et al. 2022) and *HEASOFT* v6.33.2. We selected a circular region with a radius of  $90''$  for source extraction. Background subtraction was not performed as suggested due to the high count rate of the source (Di Marco et al. 2023).

The source events in the 2–8 keV energy range are selected using *xpselect*. To conduct a model-independent polarimetric analysis, polarization cubes are generated using the *PCUBE* algorithm in *IXPEOBSSIM*. Furthermore, we produced the Stokes parameters spectra —  $I$ ,  $Q$ , and  $U$  — using the *PHA1*, *PHA1Q*, and *PHA1U* algorithms, respectively. The Stokes  $I$  spectra are grouped to ensure a minimum of 30 counts per bin, while a constant energy binning with a bin size of 0.2 keV is applied to the Stokes  $Q$  and  $U$  spectra to facilitate spectro-polarimetric analysis in *XSPEC* (Arnaud 1996).

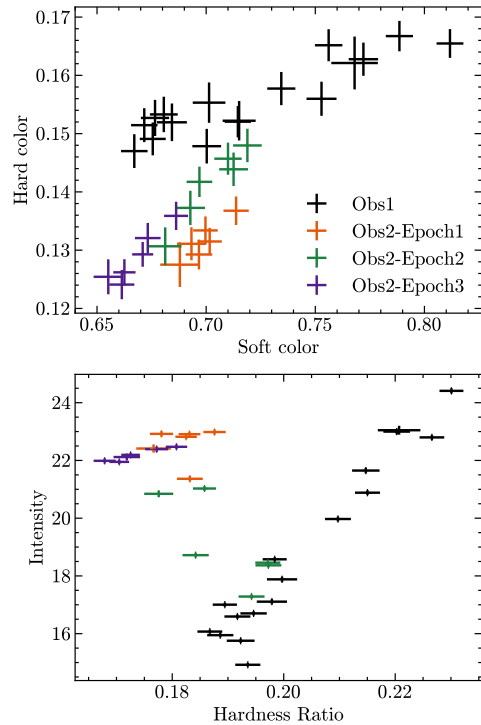


**Figure 1.** CCD (top) and HID (bottom) of XTE J1701–462 constructed using the *IXPE* data. The color or hardness is defined as the ratio of count rate in two bands: (3–5 keV) / (2–3 keV) for the soft color, (5–8 keV) / (3–5 keV) for the hard color, and (4–8 keV) / (2–4 keV) for the hardness ratio. The intensity is the count rate in 2–8 keV.

The Nuclear Spectroscopic Telescope Array (*NuSTAR*) (Harrison et al. 2013) conducted an observation of XTE J1701–462 that partially overlaps in time with *IXPE* Obs2. Cleaned level-2 events were extracted using the *nupipeline* routine from the *NuSTAR* Data Analysis Software (*NuSTARDAS*) package. Source events were collected from a circular region with a radius of  $60''$ , while background events were extracted from a concentric annular region from  $120''$  to  $150''$ . Energy spectra in the 3–30 keV band, where the source dominates, were generated using *nuproducts*, and rebinned to have a minimum of 30 counts per bin.

## 3. ANALYSIS AND RESULTS

### 3.1. Polarimetric Analysis

First, we performed a model-independent polarimetric analysis using the *PCUBE* algorithm. We found time-averaged PD =  $4.5\% \pm 0.4\%$  and PA =  $-37^\circ \pm 2^\circ$  in Obs1, and a nondetection in Obs2 (PD =  $0.84\% \pm 0.33\%$ ), consistent with previous results (Cocchi et al. 2023; Jayasurya et al. 2023; Yu et al. 2024).

We further conducted spectro-polarimetric analysis. Following the approach of Cocchi et al. (2023), we modeled the disk emission with *diskbb* and the transition layer emis-

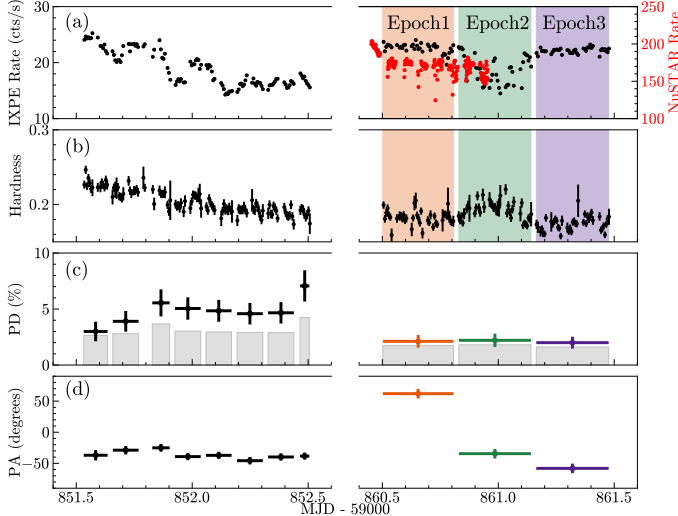


**Figure 2.** Time variation of the spectral and polarization properties. (a): *IXPE* DU1 light curve in the 2–8 keV energy range (black) and *NuSTAR* light curve in 3–30 keV (red). (b): Hardness ratio as count rate in 4–8 keV to that in 2–4 keV. (c) and (d): PD and PA in different time epochs. The gray bars mark the  $\text{MDP}_{99}$ . The three epochs in Obs2 are highlighted.

sion with `bbodyrad`. To resolve cross-calibration discrepancies, we multiplied the model spectra by  $KE^{\Delta\Gamma}$  (Zdziarski et al. 2021), and fixed  $K = 1$  and  $\Delta\Gamma = 0$  for DU1. The `polconst` model is adopted to estimate the polarization. For Obs1, the PD is found to be  $4.7\% \pm 0.3\%$  and the PA is  $-36^\circ \pm 2^\circ$ . For Obs2, the result is still a nondetection with  $\text{PD} = 0.59\% \pm 0.28\%$ . The results are consistent with those obtained with `PCUBE` within errors.

We then performed a time-resolved analysis. In each observation, we grouped the data into several segments with the same number of satellite orbits in each and assured that  $\text{PD} > \text{MDP}_{99}$  (the minimum detectable polarization at the 99% confidence level). For Obs1, where the PD is relatively high, every two orbits are grouped into a segment except the last orbit falling into a single one. For Obs2, every five orbits are grouped into a segment. The PD and PA variations as a function of time are shown in Figure 2. In Obs1, both PD and PA are consistent with a constant over time. However, in Obs2, a significant time variation of PA is observed, at  $67^\circ \pm 8^\circ$  (Epoch1),  $-34^\circ \pm 8^\circ$  (Epoch2), and  $-58^\circ \pm 8^\circ$  (Epoch3), respectively in the three epochs, while the PD remained constant at about 2%. The normalized Stokes parameters  $U/I$  and  $Q/I$  for Obs1 and the three epochs in Obs2 are displayed in Figure 3.

### 3.2. Spectral Analysis

Simultaneous *NuSTAR* and *IXPE* data are used for spectral modeling in Epoch1 and Epoch2 (no *NuSTAR* data in Epoch3), to investigate possible spectral variations associated with the observed PA variation. We began with the

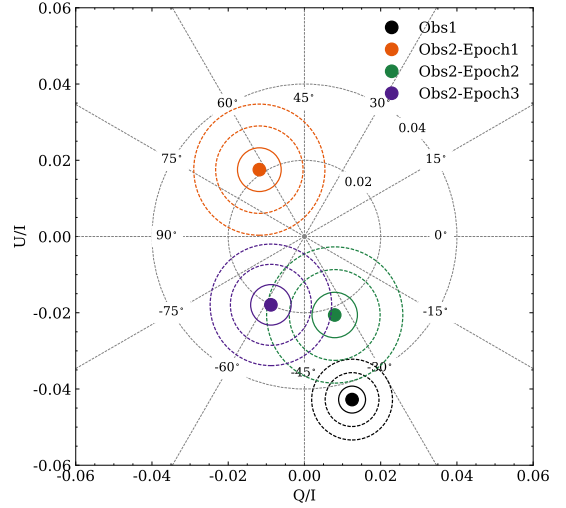


**Figure 3.** Normalized Stokes parameters  $U/I$  and  $Q/I$  over the energy range of 2–8 keV. The contours represent confidence levels at  $1\sigma$ ,  $2\sigma$ , and  $3\sigma$ .

`Tbabs` (`Diskbb` + `Bbodyrad`) model. A weak reflection feature was identified in the residuals. Therefore, we included the `RelxillNS` model (García et al. 2022) to account for reflection. In this model, we fixed the density  $\log(N/\text{cm}^{-3}) = 19$ , as the fitting result is insensitive to this parameter, the inner radius at  $R_{\text{ISCO}}$  and the outer radius at  $1000 R_g$ , the neutron star spin at 0.3, and the radial profile of emissivity at  $-3$ . The  $KE^{\Delta\Gamma}$  correction for cross-calibration issues is also included.

The best-fit spectra with model components for the two epochs are shown in Figure 4, and the spectral parameters are listed in Table 1. We also plot the data flux ratio in the same figure, as a model-independent examination of spectral variation. The ratio spectrum exhibits two bumps, one in 2–9 keV and the other in 10–30 keV, corresponding to a higher disk temperature and higher reflection in Epoch1, as one can see from model parameters. The `Bbodyrad` component remains almost the same between the two epochs.

## 4. DISCUSSIONS

We re-analyzed the archival *IXPE* observations of XTE J1701–462 during its 2022 outburst, and obtained time-averaged results well consistent with those reported in the literature (Cocchi et al. 2023; Jayasurya et al. 2023; Yu et al. 2024). However, we found that the nondetection of polarization in Obs2 was in fact due to a significant temporal variation of PA, in particular in Obs2-Epoch1, by an angle of  $76^\circ \pm 8^\circ$  with respect to Obs1,  $79^\circ \pm 11^\circ$  to Obs2-Epoch2, or  $55^\circ \pm 11^\circ$  to Obs2-Epoch3.

The PA variation is associated with spectral variation. As one can see in the CCD (Figure 1), during Obs2-Epoch1, the source follows a track distinct from the tracks in Epoch2

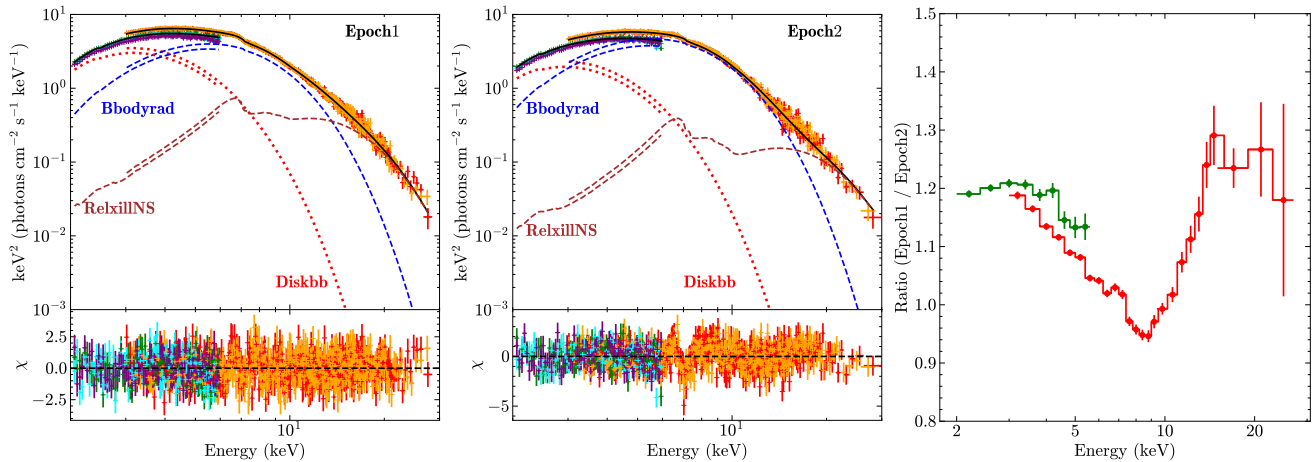


**Figure 4.** Simultaneous *NuSTAR* and *IXPE* energy spectra with best-fit models in Epoch1 (left) and Epoch2 (middle) of Obs2. The right panel displays the spectral flux ratio between the two epochs, using *IXPE* DU1 (green) and *NuSTAR* FPMA (red) data.

and Epoch3, which are along the same trend. In the HID, the source count rate in Epoch1 is also among the highest in the NB. The spectral discrepancy is clearly identified in the energy spectrum (Figure 4). Compared with the source spectrum in Epoch2, the spectrum in Epoch1 shows excesses in both the low energy (peaked around 3–4 keV) and high energy (peaked around 20 keV) bands. The former is attributed to higher thermal disk emission, while the latter is due to an enhanced reflection component in Epoch1. Also, from the spectral ratio between the two epochs, there seems to be an excessive emission line component around 6–7 keV in Epoch1, but the significance is not high.

In low magnetic systems, X-ray polarization usually reflects the geometry in radiative transfer, as the PA is perpendicular to the orientation of the last scattering direction. Thus, if the photons are scattered only once in the corona, the relative location of the seed photon and scatter determines the PA. If there are several scatters in corona, i.e., with a mean free path comparable to the corona size, the PA is perpendicular to the elongation of the corona on the sky plane, as more scatters occur along the elongation direction. Otherwise, if the optical depth is extremely high or the mean free path is much smaller than the corona size, the PA is expected to be aligned with the elongation (cf., the case of scattering plane-parallel atmosphere in Chandrasekhar 1960). We note that, in an optically thin corona, the number of scattering also depends on the energies of the seed and electron as well as the observing window, and can be greater than unity (Rybicki & Lightman 1986). Numerical simulations produce results in agreement with the first-principle estimation (e.g., Schnittman & Krolik 2010).

In the case of XTE J1701–462, emission from the accretion disk dominates the lower *IXPE* band while emission from the transition layer dominates the higher *IXPE* band.

With spectro-polarimetry, Cocchi et al. (2023) revealed an energy dependent polarization and demonstrated that the polarization signal mainly arises from emission in the transition layer instead of the accretion disk in both Obs1 and Obs2. The data in Epoch1 alone do not allow us to perform similar decomposition due to insufficient statistics. We assume that the spectral decomposition in Epoch1 is similar to that averaged in the whole Obs2, and there are a limited number of scatters in the corona (an optical depth close to unity). Then, the PA variation may have revealed a transformation of the transition layer geometry, e.g., from a slab geometry to a spreading layer geometry or vice versa. If one assumes that the X-ray PA in NS-LMXBs is generally in line with the jet orientation (Long et al. 2022; Farinelli et al. 2023), then the PA measured in Epoch1 may suggest that the corona becomes more vertically extended like a spreading layer. This naturally leads to a larger solid angle to the disk viewed by the corona, consistent with an enhanced reflection component. Such a speculation can be confirmed if the radio jet in the source can be firmly detected in the future (Fender et al. 2007; Gasealahwe et al. 2023). We note that the observed PA variation could also be due to variation in the optical depth rather than geometry, or both. However, the spectral modeling seems not in favor of a remarkable change in the corona emitting spectrum (the *Bbodyrad* component).

We acknowledge funding support from the National Natural Science Foundation of China under grants Nos. 12025301, 12103027 & 12122306, and the Strategic Priority Research Program of the Chinese Academy of Sciences.

*Facilities:* *IXPE*, *NuSTAR*

**Table 1.** Best-fit parameters for spectra in the two epochs.

Model	Parameter	Epoch1	Epoch2
Tbabs	$N_{\text{H}}$ ( $10^{22}$ cm $^{-2}$ )	$3.66^{+0.11}_{-0.09}$	$3.47^{+0.12}_{-0.14}$
Diskbb	$T_{\text{in}}$ (keV)	$0.93^{+0.13}_{-0.08}$	$0.84^{+0.06}_{-0.04}$
	$R_{\text{in}}$ (km)	$33^{+8}_{-6}$	$34^{+5}_{-4}$
Bbodyrad	$kT$ (keV)	$1.33^{+0.10}_{-0.04}$	$1.35 \pm 0.01$
	$R_{\text{bb}}$ (km)	$17^{+2}_{-3}$	$17.5^{+0.6}_{-0.3}$
RelxillNS	Emissivity	3*	3*
	$R_{\text{in}}$ ( $R_{\text{ISCO}}$ )	1*	1*
	$R_{\text{out}}$ ( $R_{\text{g}}$ )	1000*	1000*
	$a$	0.3*	0.3*
	$\log N$ (cm $^{-3}$ )	19*	19*
	Inclination (deg)	$31^{+2}_{-3}$	31*
	$\log \xi$	$2.65^{+0.18}_{-0.07}$	$2.85^{+0.16}_{-0.12}$
	$A_{\text{Fe}}$	$3.2^{+0.6}_{-0.7}$	$5.00^{+1.1}_{-0.6}$
	$kT_{\text{bb}}$ (keV)	$2.69^{+0.12}_{-0.06}$	$3.20^{+0.12}_{-0.09}$
	Norm ( $10^{-3}$ )	$2.84^{+0.26}_{-0.38}$	$1.24^{+0.14}_{-0.15}$
Cross-cal	$K_{\text{FPMA}}$	1*	1*
	$\Delta\Gamma_{\text{FPMA}}$	0*	0*
	$K_{\text{FPMB}}$	$1.01 \pm 0.01$	$1.01 \pm 0.01$
	$\Delta\Gamma_{\text{FPMB}}$ ( $10^{-3}$ )	$3.5 \pm 6.3$	$3.7^{+9.0}_{-8.6}$
	$K_{\text{DU1}}$	$0.88 \pm 0.02$	$0.95 \pm 0.03$
	$\Delta\Gamma_{\text{DU1}}$ ( $10^{-3}$ )	$16^{+21}_{-20}$	$93^{+24}_{-20}$
	$K_{\text{DU2}}$	$0.84 \pm 0.02$	$0.89^{+0.03}_{-0.02}$
	$\Delta\Gamma_{\text{DU2}}$ ( $10^{-3}$ )	$11^{+21}_{-20}$	$67^{+24}_{-21}$
	$K_{\text{DU3}}$	$0.80 \pm 0.02$	$0.78^{+0.03}_{-0.02}$
	$\Delta\Gamma_{\text{DU3}}$ ( $10^{-3}$ )	$10^{+21}_{-20}$	$-14^{+24}_{-20}$
	$\chi^2/\text{d.o.f}$	1108.95/1096	1243.54/1001
Flux ratio (2–8 keV)	$F_{\text{diskbb}}/F_{\text{total}}$ (%)	44	30
	$F_{\text{bodyrad}}/F_{\text{total}}$ (%)	51	67
	$F_{\text{relxillNS}}/F_{\text{total}}$ (%)	5	3

\* Parameters fixed in the fit.

NOTE— $R_{\text{in}}$  and  $R_{\text{bb}}$  are derived assuming a distance of 10 kpc and an inclination of  $0^\circ$ . Please refer to [Dauser et al. \(2016\)](#) for the normalization of RelxillNS.

## REFERENCES

- Arnaud, K. A. 1996, in *Astronomical Society of the Pacific Conference Series*, Vol. 101, *Astronomical Data Analysis Software and Systems V*, ed. G. H. Jacoby & J. Barnes, 17
- Baldini, L., Bucciantini, N., Lalla, N. D., et al. 2022, *SoftwareX*, 19, 101194, doi: [10.1016/j.softx.2022.101194](https://doi.org/10.1016/j.softx.2022.101194)
- Bobrikova, A., Forsblom, S. V., Di Marco, A., et al. 2024, *A&A*, 688, A170, doi: [10.1051/0004-6361/202449318](https://doi.org/10.1051/0004-6361/202449318)
- Chandrasekhar, S. 1960, *Radiative transfer*
- Cocchi, M., Gnarini, A., Fabiani, S., et al. 2023, *A&A*, 674, L10, doi: [10.1051/0004-6361/202346275](https://doi.org/10.1051/0004-6361/202346275)
- Dauser, T., García, J., Walton, D. J., et al. 2016, *A&A*, 590, A76, doi: [10.1051/0004-6361/201628135](https://doi.org/10.1051/0004-6361/201628135)
- Di Marco, A., Soffitta, P., Costa, E., et al. 2023, *AJ*, 165, 143, doi: [10.3847/1538-3881/acba0f](https://doi.org/10.3847/1538-3881/acba0f)
- Di Salvo, T., Papitto, A., Marino, A., Iaria, R., & Burderi, L. 2023, in *Handbook of X-ray and Gamma-ray Astrophysics* (eds. C. Bambi, 147, doi: [10.1007/978-981-16-4544-0\\_103-1](https://doi.org/10.1007/978-981-16-4544-0_103-1)
- Done, C., Gierliński, M., & Kubota, A. 2007, *A&A Rv*, 15, 1, doi: [10.1007/s00159-007-0006-1](https://doi.org/10.1007/s00159-007-0006-1)

- Fabiani, S., Capitanio, F., Iaria, R., et al. 2024, *A&A*, 684, A137, doi: [10.1051/0004-6361/202347374](https://doi.org/10.1051/0004-6361/202347374)
- Farinelli, R., Waghmare, A., Ducci, L., & Santangelo, A. 2024, *A&A*, 684, A62, doi: [10.1051/0004-6361/202348915](https://doi.org/10.1051/0004-6361/202348915)
- Farinelli, R., Fabiani, S., Poutanen, J., et al. 2023, *MNRAS*, 519, 3681, doi: [10.1093/mnras/stac3726](https://doi.org/10.1093/mnras/stac3726)
- Fender, R. P., Dahlem, M., Homan, J., et al. 2007, *MNRAS*, 380, L25, doi: [10.1111/j.1745-3933.2007.00350.x](https://doi.org/10.1111/j.1745-3933.2007.00350.x)
- Feng, H., Jiang, W., Minuti, M., et al. 2019, *Experimental Astronomy*, 47, 225, doi: [10.1007/s10686-019-09625-z](https://doi.org/10.1007/s10686-019-09625-z)
- García, J. A., Dauser, T., Ludlam, R., et al. 2022, *ApJ*, 926, 13, doi: [10.3847/1538-4357/ac3cb7](https://doi.org/10.3847/1538-4357/ac3cb7)
- Gasealahwe, K. V. S., Monageng, I. M., Fender, R. P., et al. 2023, *MNRAS*, 521, 2806, doi: [10.1093/mnras/stad649](https://doi.org/10.1093/mnras/stad649)
- Gilfanov, M., Revnivtsev, M., & Molkov, S. 2003, *A&A*, 410, 217, doi: [10.1051/0004-6361:20031141](https://doi.org/10.1051/0004-6361:20031141)
- Harrison, F. A., Craig, W. W., Christensen, F. E., et al. 2013, *ApJ*, 770, 103, doi: [10.1088/0004-637X/770/2/103](https://doi.org/10.1088/0004-637X/770/2/103)
- Hasinger, G., & van der Klis, M. 1989, *A&A*, 225, 79
- Homan, J., van der Klis, M., Wijnands, R., et al. 2007, *ApJ*, 656, 420, doi: [10.1086/510447](https://doi.org/10.1086/510447)
- Inogamov, N. A., & Sunyaev, R. A. 1999, *Astronomy Letters*, 25, 269, doi: [10.48550/arXiv.astro-ph/9904333](https://doi.org/10.48550/arXiv.astro-ph/9904333)
- Iwakiri, W., Serino, M., Negro, H., et al. 2022, *The Astronomer's Telegram*, 15592, 1
- Jayasurya, K. M., Agrawal, V. K., & Chatterjee, R. 2023, *MNRAS*, 525, 4657, doi: [10.1093/mnras/stad2601](https://doi.org/10.1093/mnras/stad2601)
- Lin, D., Altamirano, D., Homan, J., et al. 2009a, *ApJ*, 699, 60, doi: [10.1088/0004-637X/699/1/60](https://doi.org/10.1088/0004-637X/699/1/60)
- Lin, D., Remillard, R. A., & Homan, J. 2009b, *ApJ*, 696, 1257, doi: [10.1088/0004-637X/696/2/1257](https://doi.org/10.1088/0004-637X/696/2/1257)
- Long, K. S., Chanan, G. A., Ku, W. H. M., & Novick, R. 1979, *ApJL*, 232, L107, doi: [10.1086/183045](https://doi.org/10.1086/183045)
- Long, X., Feng, H., Li, H., et al. 2022, *ApJL*, 924, L13, doi: [10.3847/2041-8213/ac4673](https://doi.org/10.3847/2041-8213/ac4673)
- Novick, R., Kestenbaum, H. L., Long, K. S., et al. 1977, *OSO-8 X-Ray Polarimeter and Bragg Crystal Spectrometer Observations*, ed. E. A. Müller (Dordrecht: Springer Netherlands), 95–97, doi: [10.1007/978-94-010-1248-5\\_6](https://doi.org/10.1007/978-94-010-1248-5_6)
- Popham, R., & Sunyaev, R. 2001, *ApJ*, 547, 355, doi: [10.1086/318336](https://doi.org/10.1086/318336)
- Rankin, J., La Monaca, F., Di Marco, A., et al. 2024, *ApJL*, 961, L8, doi: [10.3847/2041-8213/ad1832](https://doi.org/10.3847/2041-8213/ad1832)
- Remillard, R. A., Lin, D., ASM Team at MIT, & NASA/GSFC. 2006, *The Astronomer's Telegram*, 696, 1
- Rybicki, G. B., & Lightman, A. P. 1986, *Radiative Processes in Astrophysics*
- Schnittman, J. D., & Krolik, J. H. 2010, *ApJ*, 712, 908, doi: [10.1088/0004-637X/712/2/908](https://doi.org/10.1088/0004-637X/712/2/908)
- Shakura, N. I., & Sunyaev, R. A. 1988, *Advances in Space Research*, 8, 135, doi: [10.1016/0273-1177\(88\)90396-1](https://doi.org/10.1016/0273-1177(88)90396-1)
- Soffitta, P., Baldini, L., Bellazzini, R., et al. 2021, *AJ*, 162, 208, doi: [10.3847/1538-3881/ac19b0](https://doi.org/10.3847/1538-3881/ac19b0)
- Suleimanov, V., & Poutanen, J. 2006, *MNRAS*, 369, 2036, doi: [10.1111/j.1365-2966.2006.10454.x](https://doi.org/10.1111/j.1365-2966.2006.10454.x)
- Ursini, F., Gnarini, A., Capitanio, F., et al. 2024, *Galaxies*, 12, 43, doi: [10.3390/galaxies12040043](https://doi.org/10.3390/galaxies12040043)
- van der Klis, M. 1989, *ARA&A*, 27, 517, doi: [10.1146/annurev.aa.27.090189.002505](https://doi.org/10.1146/annurev.aa.27.090189.002505)
- Weisskopf, M. C., Soffitta, P., Baldini, L., et al. 2022, *Journal of Astronomical Telescopes, Instruments, and Systems*, 8, 026002, doi: [10.1117/1.JATIS.8.2.026002](https://doi.org/10.1117/1.JATIS.8.2.026002)
- Yu, W., Bu, Q., Doroshenko, V., et al. 2024, *arXiv e-prints*, arXiv:2401.02658, doi: [10.48550/arXiv.2401.02658](https://doi.org/10.48550/arXiv.2401.02658)
- Zdziarski, A. A., Jourdain, E., Lubiński, P., et al. 2021, *ApJL*, 914, L5, doi: [10.3847/2041-8213/ac0147](https://doi.org/10.3847/2041-8213/ac0147)